High Viscous Oil–Water Two–Phase Flow: Experiments & Numerical Simulations

Archibong Archibong-Eso[a,b], Jing Shi[a], Yahaya D. Baba[a,c*], Aliyu M. Aliyu[d], Yusuf O. Raji[e], Hoi Yeung[a]

[a] Oil and Gas Engineering Centre, Cranfield University, Cranfield, United Kingdom
[b] Energy and Fluids Engineering Group, Department of Mechanical Engineering, Cross River University of Technology, Calabar, Nigeria
[c] Department of Chemical/Petroleum Engineering, Afe Babalola University, PMB 5454, Ado-Ekiti, Nigeria
[d] Faculty of Engineering, University of Nottingham, NG7 2RD, United Kingdom
[e] Chemical Engineering Programme, Abubakar Tafawa Balewa University, PMB 0248, Bauchi, Nigeria

Abstract

An experimental study on viscous oil-water two-phase flow conducted in a 5.5 m long and 25.4 mm internal diameter (ID) pipeline is presented. Mineral oil with viscosity ranging from 3.5 Pa.s – 5.0 Pa.s and water were used as test fluid for this study. Experiments were conducted for superficial velocities of oil and water ranging from 0.06 to 0.55 m/s and 0.01 m/s to 1.0 m/s respectively. Axial pressure measurements were made from which the pressure gradients were calculated. Flow pattern determination was aided by high definition video recordings. Numerical simulation of experimental flow conditions is performed using a commercially available Computational Fluid Dynamics code. Results show that at high oil superficial velocities, Core Annular Flow (CAF) is the dominant flow pattern while Oil Plug in Water Flow (OPF) and Dispersed Oil in Water (DOW) flow patterns are dominant high water superficial velocities. Pressure Gradient results showed a general trend of reduction to a minimum as water superficial velocity increases before subsequently increasing on further increasing the superficial water velocity. The CFD results performed well in predicting the flow configurations observed in the experiments.

Keywords: CFD, Flow Patterns, Pressure Gradient, Pipelines, Heavy Oil, Viscosity, Oil and Gas.

1

Corresponding author email: y.baba9550@gmail.com

1 Introduction

1.1 Background

Water usually accompanies crude oil during production especially during enhanced recovery when water is deliberately injected into older or marginal wells to aid production. In some cases, water is added for lubrication as this reduces pumping requirements for crude transport in cases where heavy or highly viscous oils are involved. Based on the above premise, the study of oil-water flow is therefore essential for production systems design and crude oil pipeline transport networks. Concurrent flow of oil and water results in a wide variety of flow patterns depending on the conditions during transportation.

The continuous depletion of light (conventional) oil reserves due to long term production has in recent years, increased the attractiveness of unconventional fossil fuels (e.g. shale gas, shale oil and especially heavy oil). Heavy oil, defined as a petroleum liquid with API gravity of <22° and viscosity >100 cP, has generated so much interest due to its huge reserves. The literature is awash with studies of light oils, but scarce in the case of heavy oils. However due to significant differences in rheological characteristics between light and heavy oils, research into the production and transportation of heavy oils has thus become important. As stated earlier, water is used to assist the flow of highly viscous oils and hence the study of the flow patterns, pressure gradients, and other characteristics is imperative for heavy oil–water liquid–liquid flows.

1.2 Previous works

Bannwart et al. [1] studied flow patterns in high viscous oil-water two-phase flow in a 0.0284 m ID, 5.43 m long glass pipe. Oil with viscosity of 0.488 Pa.s was used in the study.

Corresponding author email: y.baba9550@gmail.com

2

Superficial velocities for oil and water were 0.07 – 2.5 m/s & 0.04 – 0.5 m/s respectively. Flow patterns observed in the horizontal test section are the stratified, bubbly stratified, dispersed bubbles and annular flows. In stratified flow pattern, the upper walls of the glass pipe were observed to be constantly lubricated by water; this was attributed to interfacial phenomena and wettability effect. The bubbly stratified flow was intermittent in nature and had characteristic packages of coalesced bubbles. Homogenously dispersed bubbles in a continuous water phase were observed in the study; and the flow pattern was named the dispersed bubble flow. The annular flow pattern was observed to have a smooth and centered or wavy and off centered annulus of oil enveloped by a water phase.

Vuong et al. [2] studied high viscosity oil/water flow in horizontal and vertical pipes. Refined mineral oil ND 50 with viscosity 0.44 – 0.10 Pa.s and Tulsa City tap water were used as test fluids. The test section consisted of a U-shaped, stainless steel pipe inclined at angles ranging from -2 – 90° to the vertical with 0.0525 m ID and length of 44 m. Graduated cylinders, high speed video camera and differential pressure transducers were used to determine the water holdup, flow regimes and pressure gradients in the study. Oil and water superficial velocities ranged from 0.1 – 1 m/s for both horizontal and vertical flows. Four main flow regimes were observed in the horizontal flow test: Stratified Wavy with Oil Droplets at Interface; Dispersion of Oil in Water over a Water Layer flow; Dispersion of Oil in Water; and Dispersion of Oil in Water with Oil Film at the pipe walls. They also noted that pressure gradient was mainly influenced by flow patterns, flow rates and liquid viscosity.

Poesio et al. [3] studied two phase oil-water flow in a horizontal plastic pipeline with internal diameter of 50 mm. Oil and water viscosities used in the studies were 0.9 Pa.s (20°C) and 0.001 Pa.s respectively. Superficial oil and gas velocities ranged from 0.13 –

Corresponding author email: y.baba9550@gmail.com

0.52 m/s and 0.04 – 0.85 m/s respectively. For the low superficial velocities, flow patterns observed were the oil in water dispersion; and mixture of oil in water dispersion with bubbly flow. For the medium oil superficial velocities; three flow patterns were identified: a combination of oil in water dispersion and bubbly flow, a combination of Core Annular Flow (CAF) and oil in water dispersion; and the CAF. At high oil superficial velocities, a combination of CAF and oil in water dispersion; CAF; and the fully eccentric CAF flow patterns were observed. The authors presented the pressure gradient measurement in terms of Reduction Factor, R defined as the ratio of the pressure drop of the two-fluid flow and the pressure drop calculated using the Hagen Poiseuille law for the single-phase laminar flow of oil having the same flow rate as the oil phase in the two-phase case. They stated that R gave maximum values when CAF was observed and this was attributed to the sharp decrease in oil fouling of the pipe walls.

Sridhar et al. [4] conducted an experimental study and model assessment on high viscosity oil/water flows using the same facility as Vuong et al. [2]. Test fluid used was ND 50 with viscosity of 0.223 Pa.s and water with viscosity of 0.001 Pa.s. Superficial velocities for oil and water were 0.1 – 1 m/s and 0.1 – 0.5 m/s respectively. Test was conducted at temperature range of 60 – 100 F. Flow patterns observed included; Stratified Wavy Flow, Stratified Wavy with Dispersed Oil Droplets at Interface & Oil Film Stratified Wavy with Dispersed Oil Droplets at Interface (SOW&DO/W) and Core Annular Flow with Oil Film Core Annular Flow (CA). This flow regime was observed at increased water flow rates. Oil film was not observed at the pipe walls and the core was asymmetric. For the range of experimental data and inclination angle, there was no significant change in the flow patterns observed. The study also concluded that pressure gradient is a function of oil viscosity and flow pattern in oil-water two phase flows.

Corresponding author email: y.baba9550@gmail.com

Wang et al. [5] studied the flow characteristics of heavy crude oil-water two-phase flow in a 0.0254 m pipe ID with length of 50 m. Oil viscosity used was 0.6 Pa.s. In their study, five flow patterns were observed, water-in-oil emulsion dispersed flow (EW/O), intermittent flow of (EW/O) and partial segregated water layers, EW/O with water stratified flow, EW/O and water semi-annular flow and EW/O and water annular flow. Oil in water emulsion was present for all the flow conditions investigated. For water cut below 50% and low mixture velocities, a flow pattern in which water was dispersed in oil (DW/O) was observed. The oil's high viscosity was observed to retard the film drainage between dispersed drops thereby reducing coalescence. An increase in the mixture velocity at low water cut saw a transitions from DW/O to DW/O with partial segregated water flow. Pressure gradient in the low water cut flow patterns generally increased with in-creasing water fraction but decreased when the water in flow segregated and formed a layer. At high water fractions (>50%), oil water emulsion was not formed

Rodriguez and Baldani [6] conducted experiments on two phase liquid-liquid flows using a 15.5-m long borosilicate glass pipe with 0.026 m ID. Oil and water viscosities used were 0.28 Pa.s and 0.001 Pa.s respectively. The mixture velocities ranged from 0.13 − 0.15 m/s and water cut from 40 − 83%. Pressure gradient and holdup data were collected and analyzed in the study with emphasis on the stratified flow pattern. Commercial CFD code, ANSYS CFX was used to simulate a simplified liquid-liquid pipe flow with no interfacial dispersion. Numerical simulation in the study captured the interfacial waves observed in experimental video recordings and images. Generally, the qualitative and holdup predictions of the CFD code were good however; the pressure gradient predictions were inaccurate.

Corresponding author email: y.baba9550@gmail.com

From the aforementioned review, it is seen that oil-water flow studies using high viscosity oils were mostly carried out for oil viscosities not exceeding 1.0 Pa.s, the present work will experimentally investigate oil-water two-phase flow for oil viscosities ranging from 0.75 – 5.0 Pa.s. Additionally, only Rodriguez and Baldani [6] carried out numerical simulations of experimental results to assess the performance of commercial code, in this work, numerical simulation of flow patterns of some of the flow conditions will be presented in other to evaluate the performance of a commercially available code.

2   Experimental setup

2.1   Test Facility Description

A test facility consisting of a 5.5-m long and 0.0254-m (1 inch) internal diameter pipe fabricated from Perspex material is used in this study. The test facility's observation and measuring instruments are placed at a distance of at least 100 pipe diameters from the water and oil injection points into the main test section. This is done to facilitate complete flow development.

A progressive cavity pump (PCP) with capacity of 2.18 m^3/hr. is used to pump water through the test facility. Water volumetric flow rate is metered using an electromagnetic meter manufactured by Endress+Hauser, Promag 50P50 D50, with a range of 0 – 2.18 m^3/hr. Water is injected into the test facility through a vertically connected Tee section upstream of the main test line about 110 pipe diameters from the viewing sections.

Oil is stored in a 0.15 m^3 tank capacity manufactured from plastic material and insulated with fibres on the periphery. A variable speed PCP with maximum capacity of 0.72 m3/hr, is used in pumping oil while Endress+Hausser's Promass 83I DN 50 (Coriolis flowmeter) with

6

Corresponding author email: y.baba9550@gmail.com

range, 0 – 180 m3/hr, is used in oil metering and is capable of displaying three outputs; mass flowrate, density and viscosity. Data collection is done through a Labview data acquisition system with a HART output of 4 – 20 mA. Two main unit operations equipment used in the flow loop include separators and temperature controller. The separator is a rectangular shaped tank with viewing windows to allow for liquid level and separation process monitoring, and an internal partition with weir for overflow. Initial separation by gravity takes place in the first stage separator where the denser phase settles at the bottom while the dense phase moves to the second stage separator for further separation. A mixture of oil and water requires a residence time of at least 12–18 hours for complete separation into its component phases. On complete separation of the phases, oil is recovered and reused.

The temperature controller for oil and water is a refrigerated bath circulator manufactured by Thermo Fisher Scientific®. Copper coils submerged in the oil and water tank are connected to the circulator; by running cold or hot glycol in the coils for a certain period of time, the temperature of oil and water in the tank can be controlled based on heat transfer. The circulator temperature ranges from -5 to +50 0C. To ensure equitable temperature of the oil, a recirculation flow for about 15 minutes is carried out. Two GE Druck pressure transducers, PMP 1400, with pressure range 0–4 barg and accuracy 0.04 % over the full scale is used to obtain the static pressure in the test section. The transducers are placed 2.17 m apart. A differential pressure transducer, Honeywell STD120, with minimum pressure drop measurement of 100 Pa and accuracy of ± 0.05 % is used to measure the differential pressure. J-type thermal couples with accuracy of ± 0.1 0C placed at different locations were used in measuring the test fluid temperature. Data acquired from the

7

Corresponding author email: y.baba9550@gmail.com

flowmeters, differential pressure transducers, pressure transducers and temperature sensors are saved to a Desktop Computer using a Labview® version 8.6.1 based system.

The system consists of a National Instruments (NI) USB-6210 connector board interfaces that output signals from the instrumentation using BNC coaxial cables and the desktop computer. Three Sony camcorders, DSCH9 with 16 megapixels, high definition and 60 GB HDD are used for video recordings during the test to aid visual observations. The test facility schematic is shown in Fig. 1 below.

2.2   Test Materials

CYL 680, a mineral oil manufactured by TOTAL and water were used as the test fluids in this study. Physical properties of the test fluids are shown in Table 1.

2.3   Test Matrix

In this work the oil and water superficial velocities varied from $0.06 - 0.6$ and $0.03 - 1.0$ m/s respectively. Viscosity of the mineral oil used as the high viscosity liquid phase ranged from $3.40 - 5.10$ Pa.s.

3   Description of **CFD** Model

Numerical modeling of high viscous oil-water flow was performed using the commercial CFD code ANSYS Fluent Version 14.5 [7]. In multiphase flow systems simulations, two main techniques are generally employed: The Eulerian-Eulerian and the Eulerian-Lagrangian. In the later, the technique involves coupling the Eulerian model with a particle model while in the former, the phases in flow are mathematically analyzed as interpenetrating continua and the concept of phasic volume fraction is introduced. Volume of Fluid (VOF), Eulerian

Corresponding author email: y.baba9550@gmail.com

and the mixture model (suspension, algebraic-slip and drift-flux) are some examples of the existing Eulerian-Eulerian models in Fluent.

The Volume of Fluid (VOF) multiphase model is best suited for the surface tracking of two or more immiscible fluids with the interfacial position being a key point of interest and especially considering the hydrodynamics of the two phase oil-water flow in this study (Ghosh et al. [8]; Kaushik et al., [9]). The VOF method treats all phases as continuous, but does not allow the phases to be inter-penetrating.

3.1 Governing Equations

In the VOF model, a single set of momentum equations is shared by the two fluids. The key assumptions made in this model are: the flow is unsteady, immiscible liquid pair, isothermal, no mass transfer and no phase change.

The governing equations are:

- Continuity Equation:

$$\frac{\partial(\rho)}{\partial t} + \nabla \cdot (\rho u) = \sum_n S_n \tag{1}$$

where ρ, u, t, S and n are the density, velocity, time, mass source and the fluid type respectively. The mass source for this set up is considered to be zero based on initial assumption of no mass transfer.

- Momentum Equation:

$$\frac{\partial(\rho u)}{\partial t} + \nabla \cdot (\rho u \cdot u) = \nabla p + \nabla \cdot [\mu(\nabla u + \nabla u^T)] + \rho g + F \tag{2}$$

where ρ, u, t, p, μ, g and F are the density, velocity, pressure in the flow field, viscosity, acceleration due to gravity and the body force respectively. The body force

Corresponding author email: y.baba9550@gmail.com

3.2 Phase Tacking

Interfacial tracking of the primary (water) and secondary (oil) phases is accomplished by finding the solution of the conservation equation for secondary phase. If the volume fraction of the secondary phase is denoted by α_o, then the conservation equation is given by:

$$\frac{\partial(\rho_o a_o)}{\partial t} + \nabla \cdot (\rho_o a_o u) = 0 \qquad (3)$$

The phase volume fraction has a value of 1 when a computational cell (control volume) is entirely filled with the secondary phase, a value of 0 when the cell is void of the secondary phase and a value between 0 and 1 if an interface is present in the computation al cell. It is noted that the phase volume fraction does not uniquely identify the interface. The volume fraction of the primary phase is computed from the relationship:

$$\alpha_o + a_w = 0 \qquad (4)$$

3.3 Fluid Property estimation

Properties of the fluid in each computational cell are determined from the volume fraction of the different phases in the cell's domain. For a two-phase oil-water flow as in the case of this study, the physical properties of the fluid in a computational cell can be defined as:

$$\rho = \alpha_o \rho_o + a_w \rho_w \qquad (5)$$

$$\mu = \alpha_o \mu_o + a_w \mu_w \qquad (6)$$

3.4 Wall Adhesion and Surface Tension

The Continuum Surface Force (CSF) proposed by Brackbill et al [10] is used to model the surface tension whose effect on the flow is included in the VOF model. A resultant source term is included in the momentum equation as a result of adding the surface tension to the VOF model computation. If the surface curvature is measured by two radii, R_1 and R_2, orthogonally

Corresponding author email: y.baba9550@gmail.com

and the coefficient of the surface tension is given by σ, the pressures on either sides of the surface is given by P_1 and P_2, then the pressure drop across the surface is deduced based on the Young-Laplace equation as:

$$P_2 - P_1 = \sigma \left(\frac{1}{R_1} + \frac{1}{R_2} \right) \tag{7}$$

If α_q is the volume fraction of the q_{th} phase of the multiphase flow, the CSF model of the surface curvature is computed from the local gradients of the surface normal to the interface. If n depicts the surface normal, then it can be expressed as (Fluent Theory Guide for Version 14.5 [7]):

$$n = \nabla \alpha_q \tag{8}$$

The curvature k can be defined in terms of the divergence of the unit normal, $\hat{n}$ thus:

$$k = \nabla \hat{n} \tag{9}$$

$$\hat{n} = \frac{n}{|n|} \tag{10}$$

The surface tension can be expressed in terms of the pressure drop across the surface. The surface force can be expressed as a volume force using the divergence theorem where the volume force is the source term, F in the momentum equation. For two-phase oil-water, the source term can be expressed as:

$$F = \sigma k \frac{\rho \nabla \alpha_o}{\frac{1}{2} (\rho_o - \rho_w)} \tag{11}$$

Wall adhesion effect at the interfaces between the fluids and the rigid boundaries (pipe walls) is accounted for within the CSF model proposed by Brackbill et al. [10]

3.5 Turbulence Model

In numerical simulations of multiphase flow, turbulence models must be considered if one or

Corresponding author email: y.baba9550@gmail.com

more of the phases are in the turbulent regime. The modelling technique is used in this work. The k-ω Shear Stress Transport (SST) turbulence model which is based on the Reynolds Averaged Navier-Strokes (RANS) approach was chosen for the turbulent computations. This decision was motivated by the physics of flow, relatively low computational resources requirement and the time availability. The SST has the inherent advantage in high viscous oil-water flow; it is designed to give better prediction of the onset and the amount of flow separation under adverse pressure gradients by the inclusion of transport effects into the formulation of the eddy-viscosity. This modification results in improvements on the flow separation but is unproven in high viscosity oil-water two phase simulations (Alagbe, [11]). Menter [12] developed the SST k-ω model based on the k-ω model developed by Wilcox [13] and the free-stream independence of the k-ε model. By modifying the constant values and the turbulent viscosity to account for the transport of the turbulent shear stress; designing the blending function to be one in the near-wall and zero away from the surface thus activating the k-ω and k-ε models respectively; and introducing a cross-diffusion derivative term to the k-ω model, the SST k-ω model relatively more accurate and reliable for a wide class of applications Alagbe [11]. The model is given by:

$$\frac{\partial}{\partial t}(\rho k) + \frac{\partial}{\partial x_i}(\rho k u_i) = \frac{\partial}{\partial x_j}\left(\Gamma_k \frac{\partial k}{\partial x_i}\right) + \tilde{G}_k - Y_k + S_k \tag{12}$$

and

$$\frac{\partial}{\partial t}(\rho \omega) + \frac{\partial}{\partial x_i}(\rho \omega u_i) = \frac{\partial}{\partial x_j}\left(\Gamma_\omega \frac{\partial \omega}{\partial x_j}\right) + G_\omega - Y_w + D_\omega + S_\omega \tag{13}$$

D_ω denotes the cross-diffusion term, calculated as described below. $\tilde{G}_k$ and G_ω denotes the generation of turbulence kinetic energy due to mean velocity gradients and the generation of ω respectively. Γ_k and Γ_w represent the effective diffusivity of k and ω,

Corresponding author email: y.baba9550@gmail.com

respectively. Y_k and Y_ω represent the dissipation of k and ω due to turbulence. S_k and S_ω are user-defined source terms. The effective diffusivities for k-ω are the same as in standard k-ω model.

$$\sigma_{\omega,1} = 2.0, \sigma_{\omega,2} = 1.168, \sigma_{k,1} = 1.176, \sigma_{k,2} = 1.0 \tag{14}$$

$$a_1 = 0.31, \ \beta_{i,1} = 0.075, \ \ \beta_{i,2} = 0.0828$$

3.6 Model Geometry Design and Meshing

A three-dimensional geometry depicting the experimental test rig was created and shown in Fig 2. The pipe internal diameter (ID) is 0.0254m; a length of 5 m (around 195D) after the junction is used for the simulation. The junction is designed as a T-shaped inlet to mimic the experimental test facility. Fig. 3 shows partial meshed geometry. A dependence study was carried out using sensitivity analysis to determine the minimum mesh density that ensures that the simulation results are independent of the mesh size. After the careful study, the mesh used for the present simulations consisted of 1 197 440 hexahedral cells.

3.7 Numerical Simulation Setup

Boundary Conditions

The outlet pressure is applied at the outlet. No-slip boundary condition is implemented at the wall. Velocity inlet boundary is set up at the two inlets. Material properties are set similarly to the properties of experimental fluids. The tube is initialized with water from the water inlet at a particular superficial velocity, then both fluids are introduced at their respective inlets and the transient simulation is started. It is also worth stating that the developed flow profiles for single phase oil and water are coded loaded to the solver to ensure a full flow development at the junction. Due to its very high viscosity, oil flow is loaded as laminar while water is loaded

13

Corresponding author email: y.baba9550@gmail.com

as laminar or turbulent depending on the water flowrate for the experimental condition to be simulated. Convergence is judged based on the transport equation residuals. Besides, area-averaged static pressures and water volume fractions at various cross sections are monitored as well as mass flow rates. The hydraulic diameter and turbulence intensity are specified when implementing the turbulence model. Fluent User's Guide [7] estimates the turbulence intensity for fully developed flow, I based on the following equation:

$$I = 0.16Re^{-0.125} \tag{15}$$

where Re is the Reynolds number for the fully developed flow.

Discretization Setup

In this study, following the hydrodynamics of the two-phase flow, all simulation runs are conducted under transient conditions with time step used as the main controlling factor. The explicit VOF scheme is used. A water inlet flow condition is initialized in the solution domain. PRESTO (Pressure Staggering Option) and SIMPLE (Semi-Implicit Method for Pressure Linked Equations) are the schemes used for the interpolation of pressure and the pressure-velocity coupling respectively. First-order upwind spatial discretization scheme for momentum equation is applied first and subsequently switched to second-order upwind scheme after convergence. The interface shape is determined by the use of a Geo-Reconstruct scheme. Transient simulation with a time step of 10^{-5}s is initially used to obtain the convergence, subsequently, it is increased to 10^{-4} and 10^{-3}s with a global courant number ranging from $0.6 - 0.8$. Simulations are run until the monitored values have reached a stable solution for sufficient sampling time.

4   Results and Discussion

Results obtained from experimental investigations carried out in this study are presented in

Corresponding author email: y.baba9550@gmail.com

this section. Flow patterns and pressure gradients results are discussed, comparative analysis of pressure gradient measured with that from models in literature is also carried out, a comparative analysis of results obtained with CFD simulations for selected flow patterns are presented and finally, conclusions and contributions of this research work is stated.

4.1   Flow Patterns

In this study, high speed video camera recordings and visual observations were utilized for flow pattern identification. Six flow patterns were identified namely Water Plugs in Oil continuous phase (WPO), Rivulet, Stratified Wavy Flow (SWF), Core Annular Flow (CAF), Oil Plugs in Water Flow (OPW) and Dispersed Oil in Water Flow (DOW) flow. Table 2 shows representative images obtained from high speed video recordings for each of the flow patterns.

Characteristic feature of the flow patterns observed in the study are described below with pictures obtained from video recordings shown in Table 2 below:

Water Plug in Oil Flow Pattern (WPO): This flow pattern was observed at the lowest water superficial velocity in this study. WPO is characterized by an oil continuous phase with intermittent water plugs flowing at the pipe's bottom. Observably, the plugs increased in size with increase in water superficial velocity and diminished at relatively higher oil superficial velocity.

Rivulet flow (RIV) is characterized by a spiral motion of oil and water. This flow pattern was observed to be the transition flow pattern from an oil dominant to a water dominant flow.

Stratified Wavy Flow (SWF) was identified at higher water superficial velocities relative to the WPO and RIV. It is characterized by two distinct and segregated layers of oil and water with the former flowing at the top and the latter at the bottom. A further increase in water

15

Corresponding author email: y.baba9550@gmail.com

superficial velocity resulted in increased waviness of the oil-water interface. It is worthy to note that for some of the SWF flow patterns observed, especially close to the transition region, tiny oil plugs were dispersed at the top section of the pipe walls.

Core Annular Flow (CAF) pattern observed in this study was characterized by continuous oil phase flowing through the center of the pipe with water flowing at the walls and enveloping the oil phase. Higher water flow rates resulted in higher annulus a thinner oil core. The oil core was observed to be wavy, with its waviness increasing as the superficial water velocity increases.

Oil Plugs in Water Flow (OPW) was observed in the study, it is described as a flow pattern in which intermittent oil plugs flowed concurrently in continuous water phase. Oil was observed to foul the pipe walls in the form of streaks with the fouling reducing as water superficial velocity increased.

Dispersed Oil in Water Flow (DOW) was observed at the highest superficial velocities studied. The increase in superficial velocities of water relative to OPW was observed to result in fragments of oil plugs into tiny dispersed oil in a continuous water phase. Table 2 shows the flow patterns obtained in the experimental campaign of this study.

Flow patterns identified in the study were constructed on the x-y Cartesian plane. The x and y axes are assigned to water and oil superficial velocities respectively. Flow pattern obtained for each flow condition (superficial velocity of water and oil) investigated is shown in Fig. 4 and Fig. 5 below. It is important to note that nominal viscosity of 3.50 and 4.95 Pa.s were used in this study; however the maps shown are presented using the oil viscosity range recorded during the experimental test campaign for a particular oil nominal viscosity.

Corresponding author email: y.baba9550@gmail.com

From the maps shown in Fig. 4, it is observed that at the lowest oil superficial velocity in this study (0.06 m/s) and water superficial velocity of 0.035 m/s, flow pattern observed is WPO. An increase in water superficial velocity to 0.05 m/s resulted in a transition to the RIV. Beyond this to a water superficial velocity of 0.7 m/s, flow pattern observed is SWF. Additional increase in water superficial velocity saw a transition to the OPW and DOW. Similar flow behaviour is observed in Fig. 5, however, at different superficial velocities.

CAF flow was not observed at the low oil superficial velocity, this is attributed to the relatively smaller in situ oil holdup which results in the inability of the oil in the flow line to form and maintain a core. At increased oil superficial velocities, this was not the case as the oil in situ holdup were sufficient hence enabling a core formation and thus CAF. Additionally, it is observed that at higher oil superficial velocities within this experimental test matrix, CAF flow was the dominant flow pattern.

In comparison to flow patterns reported in other high viscosity oil-water studies conducted by Sridhar et al. [4] and Vuong et al. [2], it is noted that the RIV flow patterns was not observed in their studies. Additionally, Vuong et al. [2] studies over predicted the DOW flow region. For flow conditions where CAF was observed in the present study, the Vuong et al. [2] classified similar conditions DOW. The differences in flow patterns observed in the present study and the two studies referenced is attributed to the fluid physical properties especially the Oil viscosity. It is also noted that their studies was conducted a 2-inch pipe internal diameter was used in their study.

Comparatively, from both flow pattern maps of Fig 4 and 5, it is observed that as viscosity is increased from 3.4 − 3.6 Pa.s to 4.81 − 5.10 Pa.s, the CAF is observed at relatively lower oil and water superficial velocities. For the 3.4 − 3.6 Pa.s and 4.81 − 5.10 Pa.s, it is seen

Corresponding author email: y.baba9550@gmail.com

that CAF flow is first observed at oil superficial velocities of 0.15 m/s and 0.10 m/s respectively, thus indicating that an increase in oil viscosity may favour the formation of the CAF pattern within this experimental study range.

4.2 Pressure Gradient

Pressure gradient obtained in the study were plotted as functions of water cut for different oil superficial velocities and are as shown in Fig. 6 and 7 below. It is observed that the pressure gradient is a strong function of the water cut & flow patterns.

Generally, for water cut below 20% (most of which correspond to water superficial velocities less than 0.15 m/s), flow patterns observed were oil dominant, this results in increased shear on the pipe walls and thus, the relatively high pressure gradient observed for these flow conditions. As the water cut (and thus the water superficial velocity) is further increased, pressure gradient reduces as water helps to lubricate and thus reduce shear on the pipe wall.

The most significant reduction in pressure gradient is observed mostly around the CAF flow pattern region, this is attributed to water being constantly in contact with the pipe walls and thus reducing the pipe wall shear. Beyond the minimum pressure gradient, oil at the core fragments and moves in flow as either oil plugs or dispersed oil in continuous water flow (OPW and DOW respectively), this results in a gradually increasing pressure gradient due mainly to the fact that some of the dispersed oil and oil plugs are now in contact with the pipe walls and the increased flow mixture velocity results in a more turbulent flow thereby contributing to this increase.

Corresponding author email: y.baba9550@gmail.com

4.3   Comparison of Current Pressure Gradient with Previous Studies

Shi et al [16] did an extensive study of water-lubricated flow using the same experimental rig but with a different lube oil (also see Al-Awadi, [17]). They used the Colebrook–White equation (Colebrook [18]) to approximate the friction factor of single water flow in both hydraulic smooth pipes and rough pipes. For checking the consistency of the current results, the friction factors of both studies were compared, and they exhibited a similar trend. For the experimental Reynolds number range between 5000 and 35,000, the friction factor of water-lubricated transport of high-viscosity oil is reaches up to two times higher than that of single water flow. With increase of the Reynolds number hence the mixture velocity, the friction factor of the water-lubricated flow declines faster than that of single water flow. This is due to the fact that the oil fouling on the pipe wall reduces with increase in mixture velocity.

At developed water-lubricated flow conditions, increasing concentricity is established at larger oil superficial velocities, resulting in less oil contact with the pipe walls. Furthermore, a higher water velocity can flush oil fouling films on the pipe wall more effectively. As two groups of data were conducted in the same pipeline, it is suspected that the difference shown is due to different wettability of the pipe wall by the two different oils, and these results in different degrees of oil fouling. The wettability between the Perspex pipe and oils were not measured quantitatively in the present study. Nevertheless, we noticed that the oil fouling on the pipe wall was generally more severe for experiments with CYL 1000 oil. A quantitative study on the influence of wettability on the pressure gradient of water-lubricated flow is recommended for future studies.

Pressure gradient models by Bannwart *et al.* [1], Arney *et al.* [14], Joseph *et al.* [15] and

Corresponding author email: y.baba9550@gmail.com

Yusuf *et al*. [16] are evaluated against measured pressure gradient data obtained in this studies experiment. A plot of predicted pressure gradient as a function of the measured pressure gradient is shown in Fig. 8. The plot shows large disparity between the measured and the predicted pressure gradient. This discrepancy may be attributable to the large differences in viscosity between the present study and the studies in which models/correlations were based on as a result of the differences in flow patterns. Another key reason for the discrepancies is as a result of the pipeline fouling. In this study, it was observed that oil fouled the inside walls of the pipelines, for flow patterns were water was not the continuous phase, this effect was very prominent. This will ensure that the friction factor of the pipe walls will increase and hence the pressure gradient, a factor not accounted for in the pressure gradient prediction correlations evaluated, for oil-water flow in pipelines as earlier explained. This work therefore establishes a need for future experimental and theoretical work to be carried out on two-phase high viscosity oil-water flow to ensure deeper understanding of the flow hydrodynamics for a very wide viscosity range and to ensure further development of predictive models are based on this experimental dataset. This will form a framework on future research work in this field.

4.4 Comparison of CFD Simulation and Experiments

In this section, CFD simulation results for selected flow patterns are presented. Flow patterns simulated include the stratified wavy flow (SWF), the Core Annular Flow (CAF) and Oil Plugs in Water Flow (OPW). Results obtained for pressure gradient from each of the simulated flow condition is also presented.

4.5 Flow Pattern Predictions from CFD Simulation

Fig. 9 below shows predicted contour plots of oil volume fraction as well as the

Corresponding author email: y.baba9550@gmail.com

corresponding snapshots from recorded experimental videos for four different flow conditions. For a nominal oil viscosity of 5.0 Pa.s and superficial oil velocity around 0.1 m/s and at different superficial velocities, the flow patterns in the two-phase flow are reasonably predicted. Fig. 9 (a) shows the SWF with discontinuous thin water film at the top. From video recordings as shown in flow pattern map of Fig. 4, SWF was predicted. This dissimilarity may be as a result of SWF proximity to the CAF region and hence a transition.

Oil drops at the interface between the top oil layer and the bottom water layer can be observed in experiments, while these drops are not captured from the modelling. This may be as a result of the mesh density near the predicted interface not being denser; it may also be as result of VOF model limitation. The model uses the same set of momentum equations for the two phases. The present pipe mesh is made finer near the pipe wall to be suitable for the turbulence model selected and coarser away from the pipe wall to optimise computational time. Improved prediction may be attained with a finer meshing.

With an increase water superficial velocity from 0.05 m/s to 0.1 m/s, Fig. 9 (b) shows a thicker top water film and wavier interface compared to Fig. 6(a); CAF is formed and predicted. In Fig. 9 (c), at water superficial velocity of about 0.20 m/s (input water volume fraction of 0.67), fluctuations of the oil core as a whole is observed; heavy oil fouling on the internal pipe wall is seen due to oil core intermittently making contact with the pipe walls. CFD prediction is consistent with the experimental observations. The oil core is much wavier (especially at the top interface) compared to Fig. 9 (b). Additionally, a bit of oil fouling is captured. On further increasing the water superficial velocity, the oil core fragments into oil plugs as shown in Fig. 9 (d). Oil film can be seen from experimental videos, while for this condition no oil film is captured. This may be as a result of the mesh density. In general, CFD simulation gives a good prediction of the flow patterns observed in experiments.

Corresponding author email: y.baba9550@gmail.com

Similar conclusions were also made for CFD simulation comparison with experiments reported by [6] for oil viscosity of 0.28 Pa.s. This implies that the VOF model is reasonably sufficient for the prediction of flow patterns in oil-water two phase flows for oil viscosity up to 5.0 Pa.s.

4.6 Pressure Gradient Prediction from CFD Simulation

Pressure gradient results predicted from CFD simulation is shown in Table 3 below. Results show that CFD numerical simulation overestimates pressure gradient for the CAF flow pattern and underestimates pressure gradients in the SWF and OPW flow patterns. In general, unlike the flow pattern configurations, pressure gradient prediction from CFD numerical simulation gave not as much similarity when compared to the experimental measurements. Hence, more advanced numerical approaches will need to be implemented in future studies. These include the use of finer meshes near the wall for all flow rates, and for CAF flow patterns, this should be extended to cover regions of expected liquid film flow.

5   Conclusions

High viscous oil-water two phase flow has been experimentally investigated. New experimental results have been presented. Water Plug in Oil Flow (WPO), Rivulet flow (RIV), Stratified Wavy Flow (SWF), Core Annular Flow (CAF), Oil Plugs in Water Flow (OPW) and Dispersed Oil in Water Flow (DOW) were the flow patterns observed in the study. At high oil superficial velocities, CAF flow was observed to be the dominant flow pattern while the OPW and DOW were dominant at high superficial water velocities. Practically, this indicates that for heavy oil fields with low water cut, producing such fields using the CAF technology may be promising while the emulsion techniques may be promising for fields with high water cut.

Corresponding author email: y.baba9550@gmail.com

Pressure Gradient results showed a general trend of reduction to a minimum as water superficial velocity increases before subsequently increasing on further increasing the superficial water velocity. Pressure gradient predictive models found in literature were compared with present experimental dataset, huge discrepancies in were observed and a need to develop new models or modify existing ones is established. CFD numerical simulation performed moderately well in predicting the flow configurations observed in this study. However, results for the pressure gradient predictions were not as good.

Acknowledgement

Conflict of Interest Statement

On behalf of all authors, the corresponding author states that there is no conflict of interest.

Corresponding author email: y.baba9550@gmail.com

References

1. Bannwart AC, Rodriguez OMH, de Carvalho CHM, Wang IS, Vara RMO. Flow Patterns in Heavy Crude Oil-Water Flow. Journal of Energy Resources Technology. J. Energy Resour. Technol. 2004 Oct 19; 126(3); 184-189.

2. Vuong, DH, Zhang, HQ, Sarica, C, Li, M. Experimental Study on High Viscosity Oil/Water Flow in Horizontal and Vertical Pipes. Presented at SPE Annual Technical Conference and Exhibition, New Orleans, Louisiana, USA; 2009 Oct. 4-7.

3. Poesio P, Strazza D, Sotgia G. Two and Three-Phase Mixtures of Highly Viscous-Oil/Water/Air in a 50 mm ID Pipe. Journal of Applied Thermal Engineering. 2012 Dec.31; 49; 41 – 47.

4. Sridhar S, Zhang H-Q, Sarica C, Pereyra, E. Experiments and Model Assessment on High-Viscosity Oil/Water Inclined Pipe Flow. SPE Annual Technical Conference and Exhibition. Denver, Colorado, USA. 2011 Oct 30 – Nov. 2.

5. Wang W, Gong J, Angeli P. Investigation of Heavy Crude-Water Two Phase Flow and Related Flow Characteristics. International Journal of Multiphase Flow. 2011 Nov.; 37(9);1156 – 1164

6. Rodriguez OMH, Baldani LS. Prediction of pressure gradient and holdup in wavy stratified liquid–liquid inclined pipe flow. Journal of Petroleum Science and Engineering. 2012 Oct. 96(97); 140–151.

7. ANSYS Fluent, release 14.5, ANSYS Fluent Theory Guide (2012), ANSYS Inc., Canonsburg, USA.

8. Ghosh S., Das G., Das, PK. Simulation of core annular down flow through CFD – A comprehensive study. Journal of Chemical Engineering and Processing: Process

Corresponding author email: y.baba9550@gmail.com

Intensification. 2010 Nov. 49(11); 1222-1228.

9. Kaushik VVK, Ghosh S, Das G, Das PK. CFD Simulation of core annular flow through sudden contraction and expansion. Journal of Petroleum Science and Engineering. 2012 May; 86(87); 153 – 164.

10. Brackbill, J., Kothe, DB. Zemach, C. A continuum method for modelling surface tension. Journal of computational physics, 2012; 100 (2); 335 – 354.

11. Alagbe SO. Experimental and numerical investigation of high viscosity oil-based multiphase flows. PhD Thesis, Cranfield University, UK. 2014.

12. Menter FR. Two-equation eddy-viscosity turbulence models for engineering applications. AIAA Journal, 1994; 32 (8); 1598 – 1605.

13. Wilcox, DC. Turbulence modeling for CFD. Fluid dynamic measurements California; DCW industries, 1994.

14. Arney M. S., Bai R, Guevara E, Joseph, D, Liu K. Friction factor and holdup studies for lubricated pipelining—I. Experiments and correlations. International journal of multiphase flow, 1993; 19(6), 1061 – 1076.

15. Joseph D., Renardy Y. Fundamentals of two-fluid dynamics. Pt. II: Lubricated transport, drops and miscible liquids New York: Springer-Verlag.1993.

16. Shi, J., Lao, L., Yeung, H., Water-lubricated transport of high-viscosity oil in horizontal pipes:

The water holdup and pressure gradient, International Journal of Multiphase Flow 96 (2017) 70-85

17. Al-Awadi, H., 2011. Multiphase Characteristics of High Viscosity Oil PhD thesis. Cranfield University, UK.

Corresponding author email: y.baba9550@gmail.com

18. Colebrook, C.F., 1939. Turbulent flow in pipes, with particular reference to the transition

region between the smooth and rough pipe laws. J. ICE 11 (4), 133–156.

Corresponding author email: y.baba9550@gmail.com
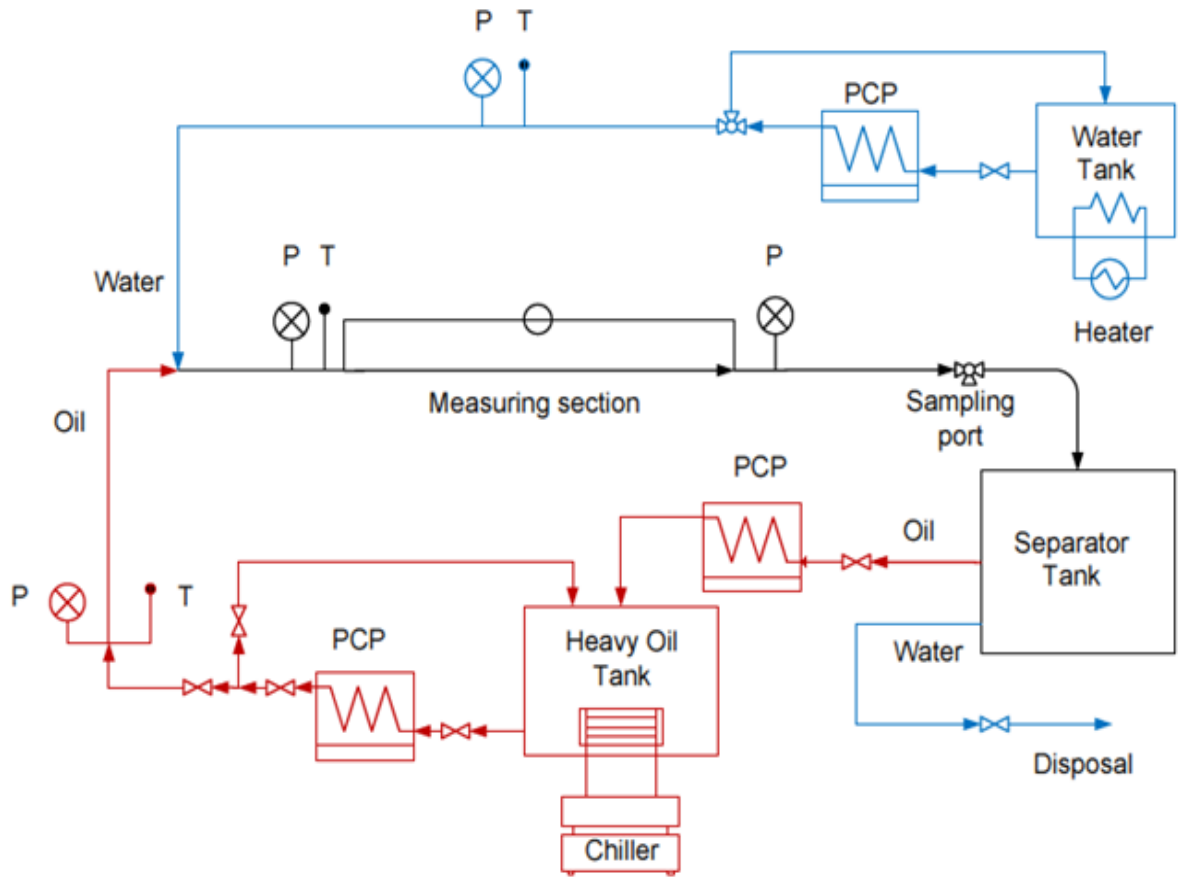
Fig. 1: Flow Schematics of the 1 inch Test Facility.

Corresponding author email: y.baba9550@gmail.com

Fig. 2: Pipe geometry for the oil-water flow simulation

Corresponding author email: y.baba9550@gmail.com
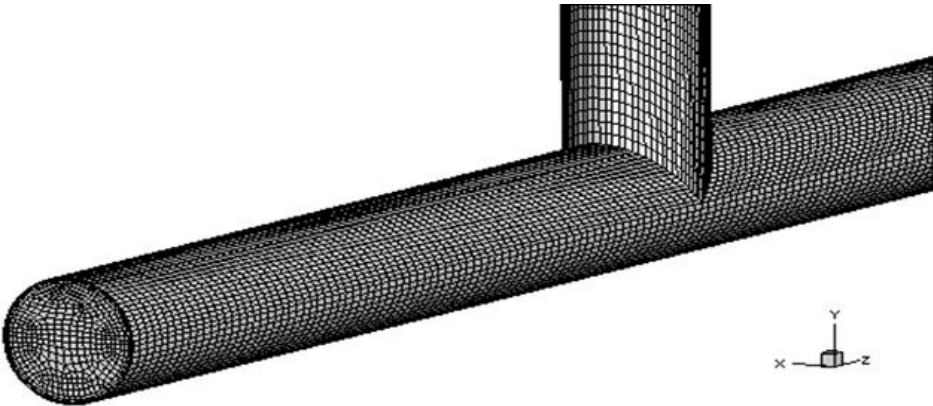
Fig. 3: Mesh for oil-water flow simulation

Corresponding author email: y.baba9550@gmail.com
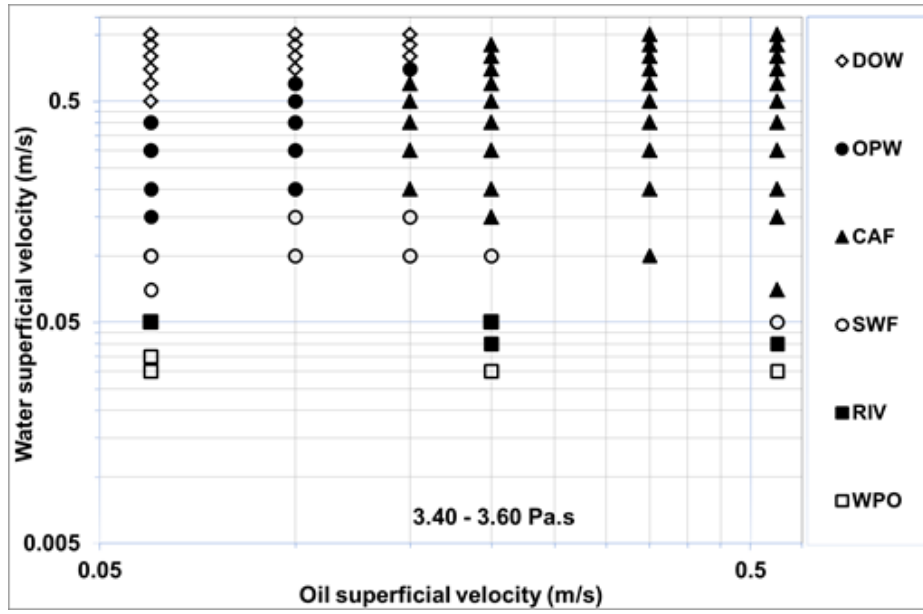
Fig. 4: Experimental flow pattern map for oil nominal viscosity of 3.5 Pa.s.

Corresponding author email: y.baba9550@gmail.com
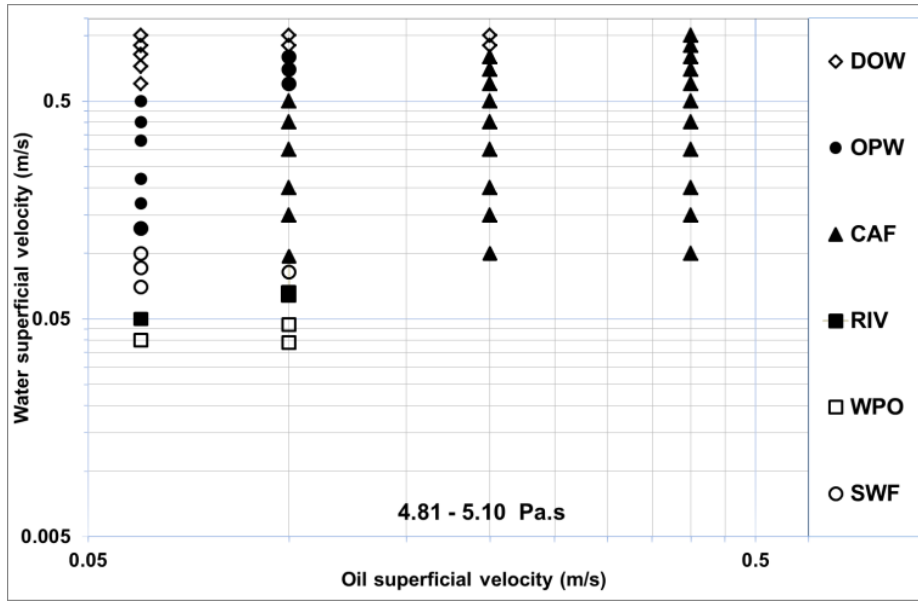
Fig. 5: Experimental flow pattern map for oil nominal viscosity of 5.0 Pa.s.
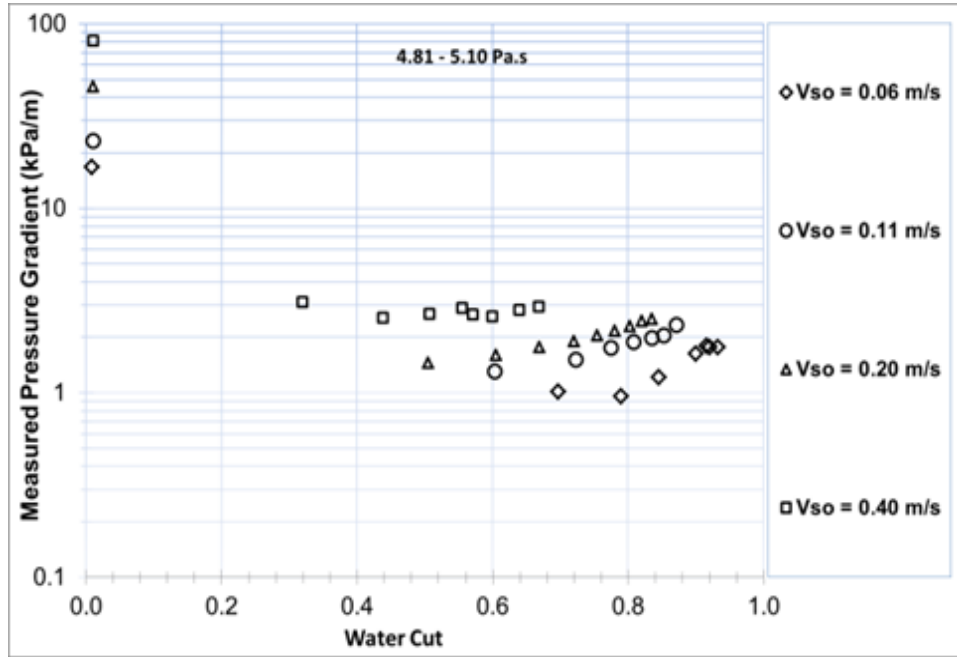
Corresponding author email: y.baba9550@gmail.com

Fig. 6. Experimental pressure gradient as a function of water cut (μ_o = 3.5 Pa.s).

Corresponding author email: y.baba9550@gmail.com

Fig. 7: Experimental pressure gradient as a function of water cut (μ_o = 5.0 Pa.s).

Corresponding author email: y.baba9550@gmail.com
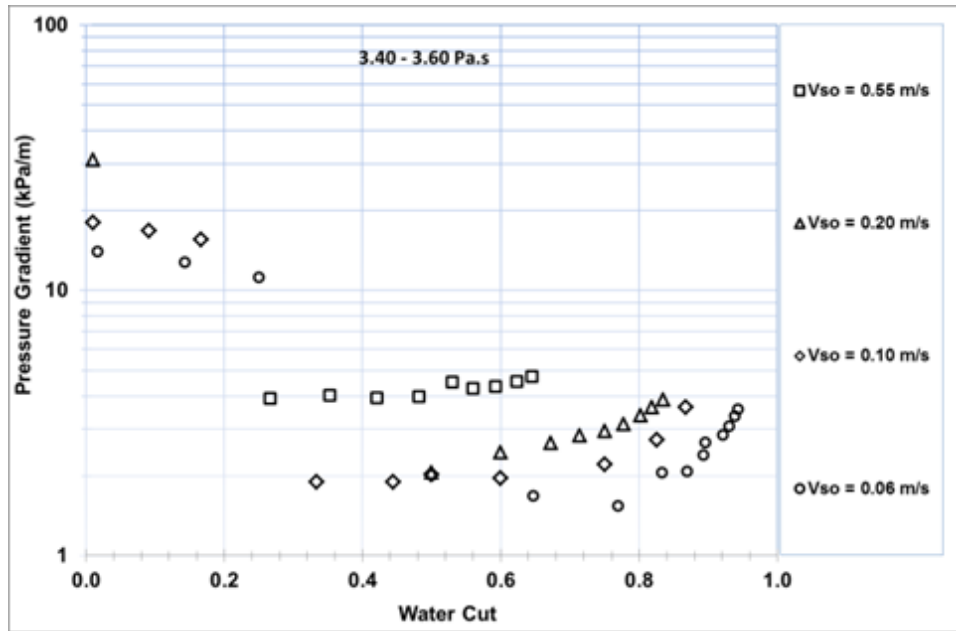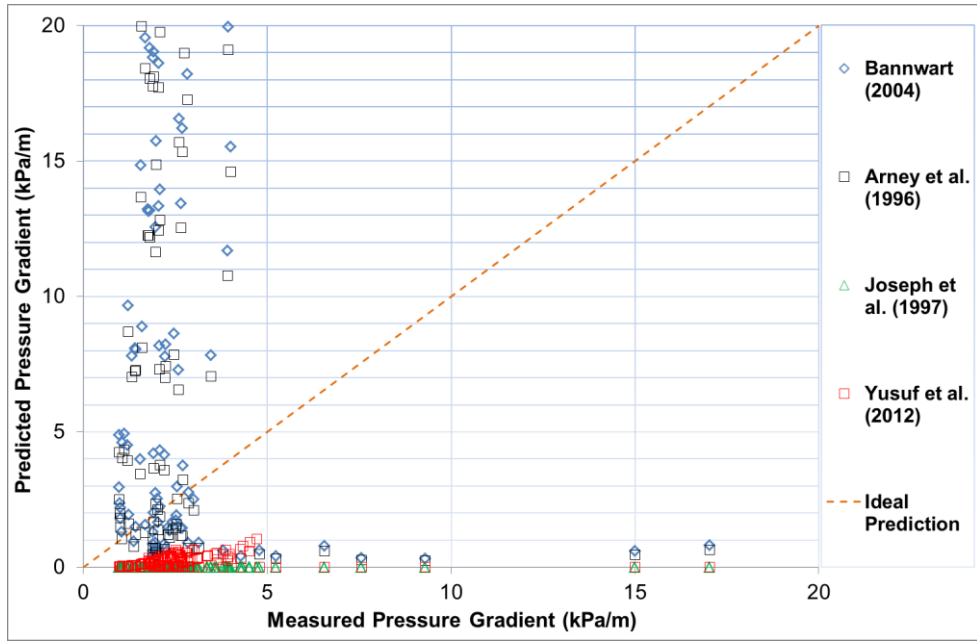
Fig. 8: Model predicted pressure gradients compared to various reported measurements.

Corresponding author email: y.baba9550@gmail.com
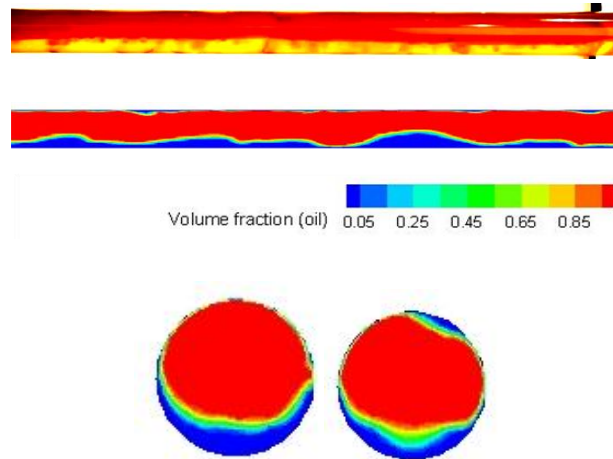
(a) Flow c condition: V_{so}=0.10 m/s, V_{sw}=0.05 m/s, μ_o=5.0 Pa.s, ρ_o=911 kg/m^3 (SWF)
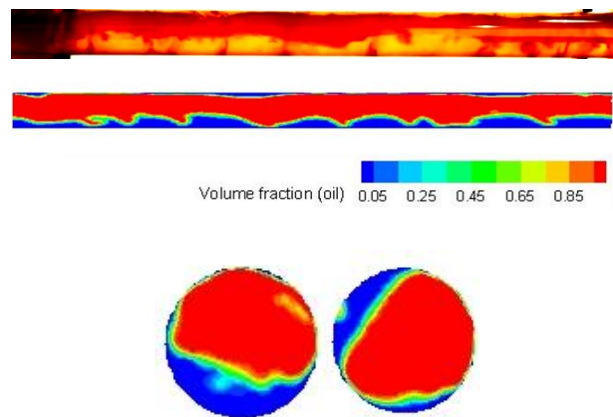
(b) Flow condition: V_{so}=0.10 m/s, V_{sw}=0.10 m/s, μ_o=5.0 Pa.s, ρ_o=911 kg/m^3 (CAF)

(c) Flow condition: V_{so}=0.10 m/s, V_{sw}=0.20 m/s, μ_o=5.0 Pa.s, ρ_o=911 kg/m^3 (CAF)

Corresponding author email: y.baba9550@gmail.com
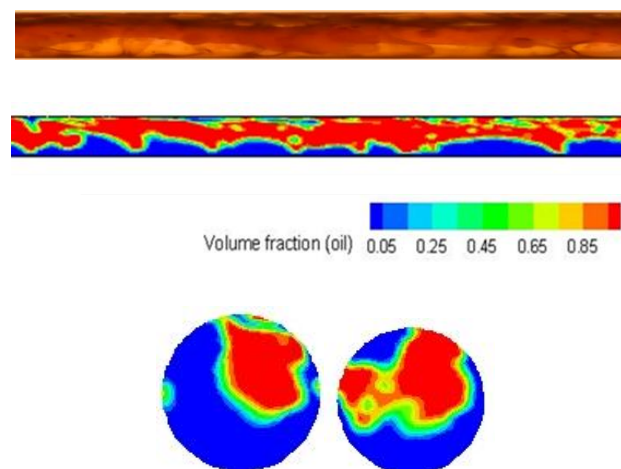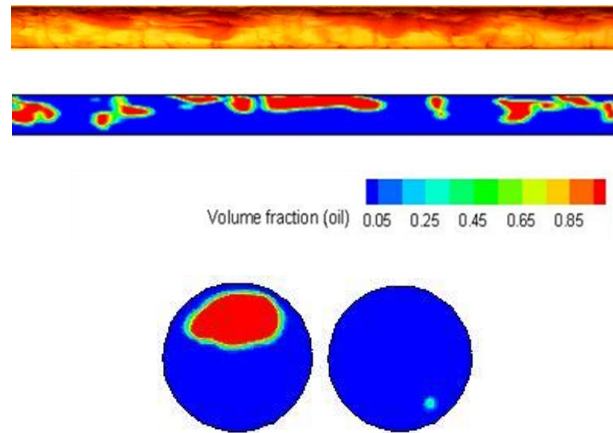
(d) Flow condition: V_{so}=0.10 m/s, V_{sw}=0.81 m/s, μ_o=5.0 Pa.s, ρ_o=911 kg/m^3 (OPW)

Fig. 9: Comparison of flow patterns in CFD simulations and experiments.

Corresponding author email: y.baba9550@gmail.com

Table 1: Physical Properties of Test Fluids

Test fluids	Density at 25 ℃ (kg/m3)	Viscosity at 25 °C (Pa.s)	Interfacial tension at 19 °C , (N/m)	API gravity
Water	≈ 998	0.00103		---
CYL680	≈ 917	1.83	0.029	22.67

Corresponding author email: y.baba9550@gmail.com
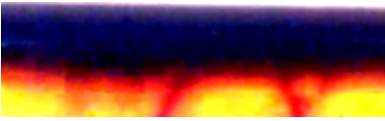
Table 2: Representative images for the observed flow patterns

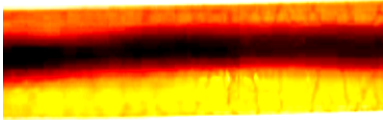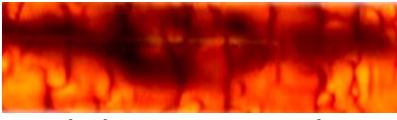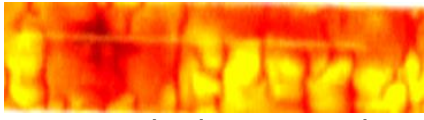**Flow Patterns**

Water Plug in Oil Flow

Rivulet Flow

Stratified Wavy Flow

Core Annular Flow

Oil Plugs in Water Flow

Dispersed Oil in Water Flow

Corresponding author email: y.baba9550@gmail.com

Table 3: Experiment and CFD Predictions for Pressure Gradient

Vso (m/s)	Vsw (m/s)	Pressure Gradient (kPa/m)		Flow Pattern
		Experiment	CFD	
0.10	0.05	1.25	1.17	SWF
0.10	0.10	1.24	1.91	CAF
0.10	0.60	1.83	0.61	OPW

Corresponding author email: y.baba9550@gmail.com